Original

Beig, G.; Fadnavis, S.; Schmidt, H.; Brasseur, G.P.:

Inter-comparison of 11-year solar cycle response in mesospheric ozone and temperature obtained by HALOE satellite data and HAMMONIA model

In: Journal of Geophysical Research (2012) AGU

DOI: 10.1029/2011JD015697

Inter-comparison of 11-year solar cycle response in mesospheric ozone and temperature obtained by HALOE satellite data and HAMMONIA model

G. Beig,[1] S. Fadnavis,[1] H. Schmidt,[2] and Guy P. Brasseur[3]

Received 25 January 2011; revised 29 October 2011; accepted 31 October 2011; published 6 January 2012.

[1] To investigate the effects of decadal solar variability on ozone and temperature in the MLT region, data obtained from the Halogen Occultation Experiment (HALOE) aboard Upper Atmospheric Research Satellite (UARS) during the period 1992–2004 are analyzed using a multifunctional regression model. The experimental results are compared with results from the 3-D chemistry climate model HAMMONIA (Hamburg Model of Neutral and Ionized Components). The simulated and observed responses of temperature and ozone profiles to the 11-year solar cycle show many similarities. The inferred annual-mean solar signal in ozone is found to be insignificant in the lower mesosphere whereas it is of the order of 5%/100 sfu (solar flux units; units of 10.7 cm radio flux) in the upper mesosphere for both low and mid latitudes. Results indicate a hemispheric symmetry in the tropics but not at midlatitudes for the ozone response. The inferred annual mean temperature response is found to be of the order of 0.5–1 K/100 sfu. There is better agreement between the HALOE derived and model simulated responses in the tropics than at midlatitudes, both in temperature and ozone. Results obtained in the present study are also compared with the results obtained by other models.

Citation: Beig, G., S. Fadnavis, H. Schmidt, and G. P. Brasseur (2012), Inter-comparison of 11-year solar cycle response in mesospheric ozone and temperature obtained by HALOE satellite data and HAMMONIA model, *J. Geophys. Res.*, *117*, D00P10, doi:10.1029/2011JD015697.

1. Introduction

[2] The analysis of temperature trends in the mesosphere and thermosphere has not been as comprehensive as in the lower atmosphere. One of the major sources of decadal natural variability in the middle and upper atmosphere is the 11-year solar activity cycle [*Brasseur and Solomon*, 1986]. Variations arising on decadal and even longer time scales, having a natural origin, may also play a significant role on long-term trend estimates. Electromagnetic flux emitted from the Sun varies at different time scales mainly in the shorter wavelengths [*Donnelly*, 1991]. Incoming solar radiation provides the external forcing for the Earth-atmosphere system. While the solar Lyman α-flux varies by a factor of about two over a solar cycle, changes in the UV (180 to 300 nm) are smaller. Several studies on the changes in solar UV spectral irradiance on timescales of the 27-day and 11-year solar cycles have been performed in the past [e.g., *Donnelly*, 1991, *Woods and Rottman*, 1997]. It is believed that the changes arising in several mesospheric parameters due to anthropogenic activities are small but continuous in nature whereas changes due to variation in solar activity are comparatively larger and periodic [*Beig*, 2000].

[3] The response of temperature and ozone to 11-year solar UV variations is difficult to isolate using satellite data. This is partially due to the short life time of satellites compared to the length of a solar cycle, and partially to space instrument drifts. On this time scale, the quasi coincidence of the recent major volcanic eruptions with solar maximum [*Kerzenmacher et al.*, 2006] conditions increases the challenge. In the past, only rocket observations have provided long temperature series in the mesosphere. However, the required aerodynamic corrections and changes of the sampling and the time of measurements induce a significant bias mainly in the upper mesosphere. From space, the Halogen Occultation Experiment (HALOE) on the Upper Atmosphere Research Satellite (UARS) is the only experiment that provides mesospheric temperature data sets over more than a decade with a single instrument. However, the number of solar occultation provides only a limited sampling.

[4] In recent time, several studies related to 11-year periodicities in the temperature of the mesosphere and lower thermosphere (MLT) region have been performed [*She and Krueger*, 2004, and references therein]. The search for the effects of the 11-yr solar cycle on middle atmosphere temperature has also been protracted and is uncertain. Model studies suggest an in-phase response to the UV-flux, peaking

[1]Physical Meteorology and Aerology Division, Indian Institute of Tropical Meteorology, Pune, India.
[2]Atmosphere in the Earth System, Max Planck Institute for Meteorology, Hamburg, Germany.
[3]Climate Service Center, Hamburg, Germany.

0148-0227/12/2011JD015697

in the upper mesosphere (2 K amplitude) and at the stratopause (1 to 2 K amplitude) [e.g., *Brasseur*, 1993; *Matthes et al.*, 2004]. However, the satellite analysis of *Scaife et al.* [2000] indicates a maximum response at low latitudes of about 0.7 K between 2 and 5 hPa, while the study of *Hood* [2004] shows a near zero response at 5 hPa but a positive response above this level increasing sharply to reach 2 K near 1 hPa. The increase of solar influence with altitude is not smooth. For example, the periodic solar effect in the mesopause region is relatively small [*Matthes et al.*, 2004]. It is therefore easier to study long-term trends in this region. It should be emphasized that, if one does not account properly for the solar cycle response; there can be biases for any remaining trend term. *Remsberg and Deaver* [2005] have analyzed long-term changes in temperature versus pressure provided by the 12.5-years time series of zonal average temperature from HALOE on the UARS. The temperature data provided by this instrument are being obtained using atmospheric transmission measurements from its CO_2 channel centered at 2.8 μm [*Russell et al.*, 1993; *Remsberg et al.*, 2002; *Hervig et al.*, 1996]. While the length of their data set is quite short (1992 – 2001) compared to the 11-year solar cycle, *Remsberg et al.* [2002] report a mesospheric response to solar variability of 2–3 K around 70–75 km.

[5] The solar response in temperature along with ozone in the MLT region has also been simulated using theoretical models. In principle, these models, which are able to account properly for the vertical coupling processes between different atmospheric layers are suitable to study solar variability effects. The number of model studies that have assessed the effect of solar variability on temperature or other parameters in the MLT region is limited compared to the number of studies focusing on stratospheric regions where a relatively large number of models have been used [*Rozanov et al.*, 2004, and references therein]. The 11-yr solar cycle variability was studied with different versions of the SOCRATES (Simulation of Chemistry, Radiation, and Transport of Environmentally Important Species) interactive 2D model by *Huang and Brasseur* [1993] and by *Khosravi et al.* [2002]. *Huang and Brasseur* [1993] reported a temperature peak-to-peak response to solar activity in the mesopause region of about 10 K whereas *Khosravi et al.* [2002] reported a value of 5 K. Only very recently, a few models have been developed to include a detailed dynamical description of the atmosphere from the troposphere to the thermosphere, with coupled comprehensive chemistry modules (GCMs with interactive chemistry are referred to as chemistry climate models, CCMs). Models of this type are the Extended Canadian Middle Atmosphere Model (EXCMAM) [*Fomichev et al.*, 2002], the Whole Atmosphere Community Climate Model (WACCM) [e.g., *Beres et al.*, 2005] and the Hamburg Model of the Neutral and Ionized Atmosphere (HAMMONIA) [*Schmidt et al.*, 2006; *Schmidt and Brasseur*, 2006] These models are arguably the most advanced numerical tools existing today to study the coupled response of chemistry and dynamics to the variability in solar irradiance.

[6] There is a great deal of uncertainty in the amplitude of temperature and ozone variability in the MLT region. Model results differ considerably with observed variations in the temperature and ozone responses to solar activity. Hence, there is a need to narrow down the uncertainty. In the present paper, an attempt is made to compute the temperature and ozone response to 11-year variation in solar activity using both observations and model simulations. For this purpose we use the subset of HALOE satellite data from January 1992 to December 2004. The observed solar response in mesospheric temperature and ozone is compared with simulation results obtained with HAMMONIA.

2. HALOE Data and Regression Analysis

[7] The vertical structure of the middle atmospheric temperature and ozone volume mixing ratio along with other species have been monitored by HALOE from October 1991 to November 2005 [*Russell et al.*, 1993; *Remsberg et al.*, 2002; *Brühl et al.*, 1996; *Hervig et al.*, 1996]. Since HALOE is a solar occultation instrument, measurements are made only during limb viewing conditions (sunrises and sunsets). Latitudinal coverage ranges from 80°S to 80°N. The UARS orbit has an inclination of 57° and a period of about 96 min. The maximum range holds only around equinox. At the solstices, data are available to about 50 degrees in the winter hemisphere and 67 degrees in the summer hemisphere. This results in the 30 profile observations per day at two quasi-fixed latitudes; i.e., 15 profiles at one latitude corresponding to sunrise and 15 at latitude corresponding to sunset. These bands are typically in opposite hemispheres. Data on temperature and ozone volume mixing ratio are taken as NETCDF files from the Website: http://haloe.gats-inc.com

[8] In this present study, in order to investigate the effects of decadal solar variability, we analyze monthly mean temperature and ozone profiles in the Northern and Southern Hemispheric tropics (0–30°N, 0–30°S) and midlatitudes (40–60°N and 40–60°S) for the period January 1992 to November 2005 and for the pressure levels from 1 hPa to 0.002 hPa i.e., an approximate altitude range of 50 to ~90 km. Sunrise and sunset data are analyzed separately for each belt (0–30°N, 0–30°S, 40–60°N and 40–60°S) to avoid tidal interference. Sunrise and sunset trends are then averaged to obtain a single trend coefficient at every pressure level. Zonally averaged, monthly mean data so obtained are used for each level in our analysis. Separating the data for sunrise and sunset reduces the number of sampling points in a month if we select a narrow band and we get 8–12 data points or less in a month. For statistical robustness, data for 15 days or more should be available each month. Hence, to maintain the statistical robustness of our analysis, we use the wider latitude bin since statistical robustness is the major issue in long-term-trend or response analyses [*Beig et al.*, 2003; *Beig*, 2002; *Weatherhead et al.*, 2002, and references therein]. This is needed to increase the homogeneity in the data set and to get enough sampling points for statistical robustness, which cannot be achieved with smaller bins. In order to remove the effects of other natural, periodic and anthropogenic signals, like the QBO, ENSO and trends, we use a regression model which is an extended version of the model developed by *Randel and Cobb* [1994]. The regression model equation is

$$\theta(t,z) = \alpha(z) + \beta(z) \times \text{Trend}\,(t) + \gamma(z) \times \text{QBO}(t) + \delta(z) \times \text{Solar}(t) + \varepsilon(z) \times \text{ENSO}\,(t) + \text{res}\,(t) \quad (1)$$

Coefficients α, β, γ, and δ are expressed by harmonic expansions. For example, the harmonic expansion for α(t) is given by:

$$\alpha(t) = A_0 + A_1 \cos \omega t + A_2 \sin \omega t + A_3 \cos 2\omega t + A_4 \sin 2\omega t + A_5 \cos 3\omega t + A_6 \sin 3\omega t + A_7 \cos 4\omega t + A_8 \sin 4\omega t \quad (2)$$

where $\omega = 2\pi/12$; A_0, A_1, A_2,… … . are constants and t (t = 1, 2 ….n) is the time index. Coefficients α, β, γ, δ and ε are calculated at every altitude for every month.

[9] For the QBO proxy, QBO(t), we use the Singapore monthly mean QBO zonal wind velocities (m/s) at 30 hPa. The Mg II Index shows good correlation with UV and EUV solar cycle variations. In addition, since the F10.7 solar radio flux and Mg II index are strongly correlated (99.9%) [*Thuillier and Bruinsma*, 2001] we used the F10.7 indices as a solar proxy (solar (t)). This index is the Ottawa monthly mean F10.7 solar radio flux. For the ENSO proxy ENSO(t), we use the Southern Oscillation Index (SOI), which is the Tahiti (18°S, 150°W) minus Darwin (13°S, 131°E) monthly mean sea level pressures (hPa). Here, α(z), β(z), γ(z), δ(z) and ε(z) represent the time-dependent 12-month seasonal, trend, QBO, solar flux and ENSO coefficients, respectively and res(t) represents the residues or noise of the regression method. Thus, the solar coefficient obtained should be free from a trend and signals produced by the QBO and ENSO. The model performs multiple regression analyses of time series at each given pressure level. According to *Neter et al.* [1985], the error estimates are represented by

$$\sigma^2(\alpha) = \left[\sigma^2(A_0) + \sigma^2(A_1)\cos^2\omega t + \sigma^2(A_2)\sin^2\omega t + \ldots .. + 2\left(\sigma(A_1, A_2)\cos\omega t + (\sigma(A_1, A_3)\sin\omega t + \ldots ..\right)\right] \quad (3)$$

[10] Here $\omega = 2\pi/12$, σ^2 (A_0) and σ(A_1, A_2) etc are variance-covariance estimates of regression coefficients, obtained from least square analysis [*Randel and Cobb*, 1994]. These errors are indicated as error bars in the vertical profiles of ozone and temperature responses to solar variability (Figures 4, 5, 6 11 and 12). For HALOE uncertainties, we refer to *Brühl et al.* [1996] and *Hervig et al.* [1996].

3. HAMMONIA Model Simulations

[11] HAMMONIA [*Schmidt et al.*, 2006] is an upward extension of the MAECHAM-5 model [*Manzini et al.*, 1997; *Giorgetta et al.*, 2002], which is itself a vertical extension to the lower mesosphere of the ECHAM-5 atmospheric general circulation model [*Roeckner et al.*, 2003, 2006]. ECHAM-5 is the most recent version in a series of ECHAM models evolving originally from the spectral weather prediction model of the European Centre for Medium Range Weather Forecasts (ECMWF) [*Simmons et al.*, 1989]. HAMMONIA also comprises a full dynamic and radiative two-way coupling with the MOZART-3 chemical module [*Kinnison et al.*, 2007] that includes 48 compounds and 148 gas phase reactions in the version used here (see *Schmidt et al.* [2006] for a listing of the full chemistry mechanism). HAMMONIA has a spectral dynamical core. The simulations analyzed here are performed with a triangular truncation at wave number 31 (T31) and with 67 vertical levels ranging from the surface to $1.7*10^{-7}$ hPa (~250 km altitude). For the computation of physics and chemistry, the spectral dynamical variables are transformed to a horizontal grid with 48 × 96 points. The advective transport of chemical compounds is performed using the semi-Lagrangian scheme of *Lin and Rood* [1996]. The dynamical and radiative processes that have been specifically implemented in HAMMONIA include solar heating in the UV and EUV wavelength regime (spectral resolution down to 5 nm [*Richards et al.*, 1994]), a nonlocal thermodynamic equilibrium long-wave radiative scheme [*Fomichev and Blanchet*, 1995; *Fomichev et al.*, 1998], heating and mixing due to parameterized gravity waves [*Hines*, 1997a; *Hines*, 1997b], vertical molecular diffusion and heat conduction (parameterized following the basic equations from *Banks and Kockarts* [1973]), and a simple parameterization of electromagnetic forces in the thermosphere (ion drag and Lorentz forces [*Hong and Lindzen*, 1976]). To assess the effect of the 11-yr solar cycle, two simulations with a length of 20 yr each have been performed. Both simulations are performed for "present-day" conditions of greenhouse gas concentrations. The first simulation represents conditions typical of a solar cycle minimum (as observed in September 1986). The second simulation refers to conditions typical of solar maximum (November 1989). The HAMMONIA output (as well as the output from other models presented for comparison) is not subjected to regression analysis. The responses of ozone and temperature to solar variability are obtained as differences of the respective fields for solar maximum and solar minimum (as shown in Figures 4–6 and 11–12) and scaled to 100 sfu by considering the solar radio flux during the period for which the simulation is performed. This is performed to facilitate a direct comparison with HALOE data. The spectral solar irradiance data used for these periods were produced by *Lean* [2000]. A more detailed description of the model experiments analyzed in the present paper is given by *Schmidt et al.* [2006]. *Dikty et al.* [2010] have compared the daylight part of the diurnal cycle in ozone and temperature as simulated by HAMMONIA with observations from the SABER instrument. In particular the ozone variations are well reproduced by the model. It may be noted here that *Austin et al.* [2008] have studied the response of ozone and temperature to solar cycles using their new simulations of coupled chemistry climate model. They state that further understanding of solar processes requires improvement in the observations of the vertically varying and column integrated ozone.

[12] In the present study, HAMMONIA results are presented as multiannual averages either for the equator (which is taken as an average of the two model latitude bands centered at ~1.9° North and South) or averaged over larger latitude bands. In the first case, only local times of 0600 h and 1800 h are considered which correspond to a zenith angle of nearly 90° all year-round and allow therefore a direct comparison to HALOE observations. In the second case, zonal averages (meaning also an averaging over local times) are presented and compared to averages of sunrise and sunset data from HALOE. A quantitative comparison is more difficult in this case since the diurnal cycle of ozone is

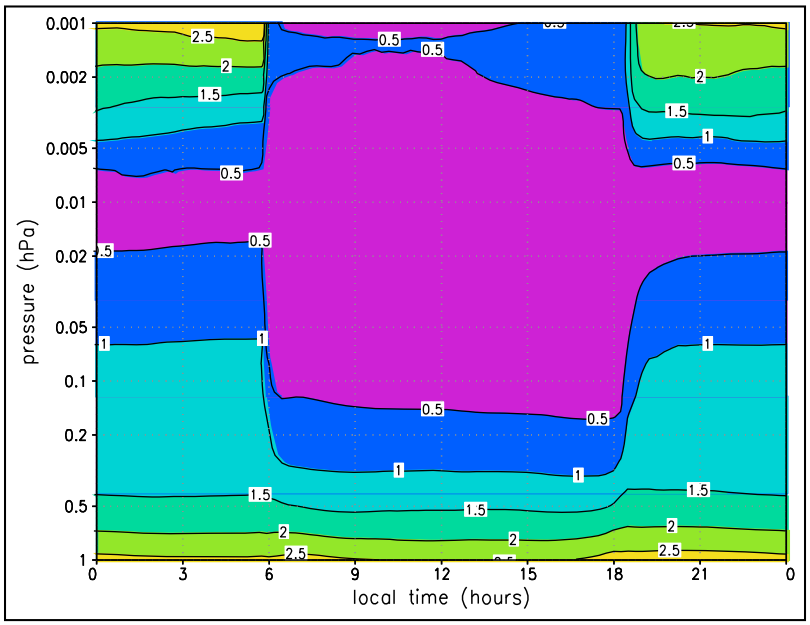

Figure 1. Diurnal variation in ozone (ppmv) at the equator as obtained from HAMMONIA model simulation.

very strong in particular in the middle and upper mesosphere (see section 4).

4. Results and Discussion

4.1. Diurnal Variation in Ozone at the Equator

[13] The output frequency used for model variables analyzed in this study is once every three hours. This means that 8 simulated values per day exist for 96 longitudes which also represent 96 local times (at a 15 min LT interval defined by the longitudinal grid). Hence, diurnal cycles presented in this study that appear to have a time resolution of 15 min, use, for each of these time steps, averages from 8 different longitudes. Figure 1 exhibits the diurnal variation in ozone volume mixing ratios (ppmv) at the equator as obtained from the HAMMONIA model simulation. Ozone exhibits a strong diurnal variation. Ozone mixing ratios are minimum (0.5ppmv) at the local time between 6–18 h at the pressure levels ranging from 0.1 hPa (~64 km) to 0.003 hPa (~88 km). During 0–6 h and 18–24 h ozone mixing ratios vary between 0.5 and 2.5 ppmv. In particular in the mesosphere, ozone photochemistry undergoes a fast transition from nighttime to daytime and vice versa at sunrise and sunset, respectively. This is why even small differences between local times in observed and simulated data could cause considerable differences between compared quantities. But, as mentioned before, at the equator, the two particular local times (0600 h and 1800 h) considered here should be very close to the times of HALOE sunrise and sunset observations independent of the time of year.

[14] Figure 2 shows the vertical profiles of differences in ozone volume mixing ratio between sunset and sunrise conditions. In the case of HALOE, the ozone volume mixing ratios are zonally averaged over the 10°S-10°N wide latitudinal belt, while in the case of HAMMONIA an average for

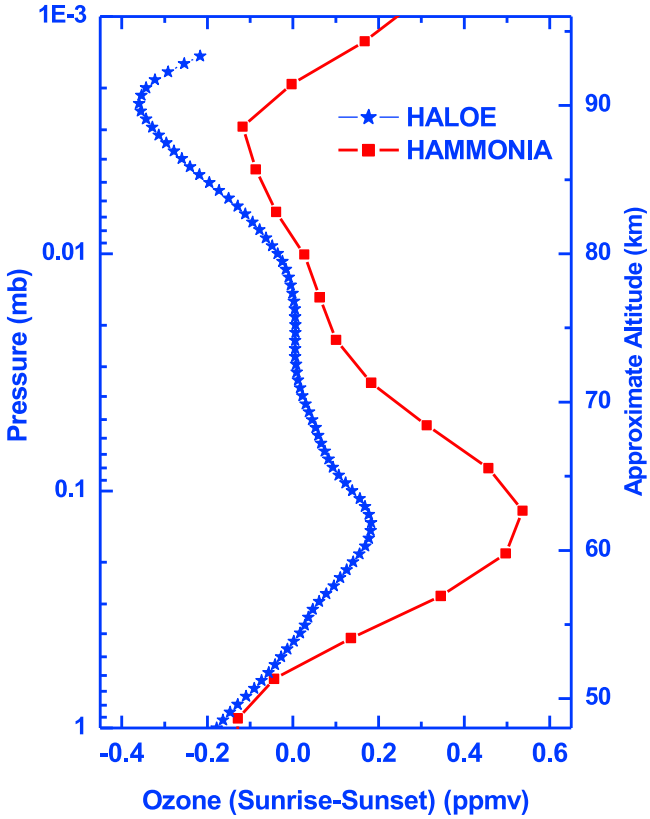

Figure 2. Comparison between the diurnal variation of ozone (sunrise–sunset) simulated by HAMMONIA at the equator and the average ozone volume mixing ratio observed by HALOE in the 10N-10S latitudinal belt.

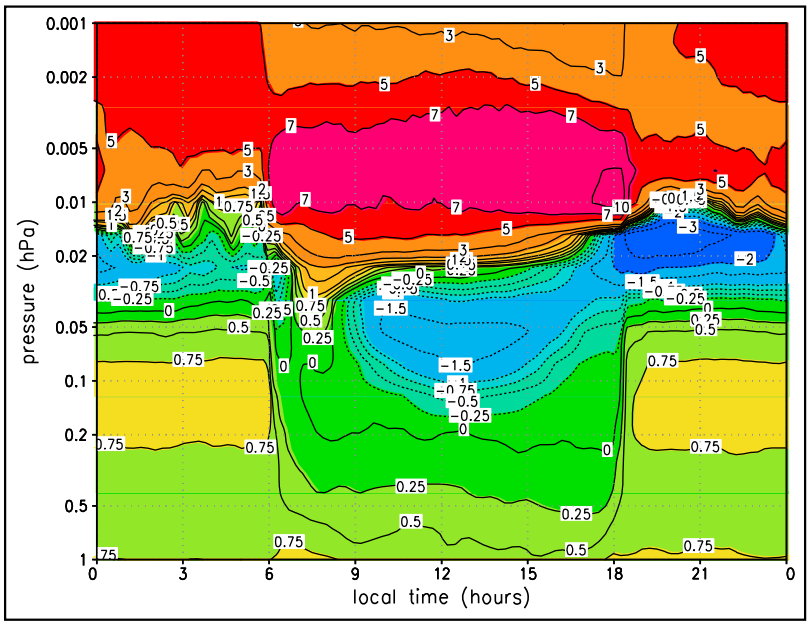

Figure 3. Solar response (%/100 sfu) of the diurnal variation of ozone at the equator obtained from HAMMONIA.

the model latitudes just south and north of the equator is used (see above). It is quite evident that both profiles exhibit similar shapes, and in most cases qualitative agreement is good. However, the quantitative agreement is poor at some altitudes. At the 1 hPa pressure level, the difference is small (0.2 ppmv), but it increases with height and reaches a maximum near 0.1 hPa. The amplitude of diurnal variation derived from HALOE is lower than that produced by HAMMONIA. It is difficult to speculate about the reason for these differences. The comparison, however, is not made for exactly the same conditions. As mentioned before, observed and simulated values are taken from latitude bands of different width, and the local times of observation and simulation do not match exactly. While the absolute uncertainty arising from this approach is difficult to quantify, we expect them to contribute only weakly to the differences. One known deficiency of the model is that it allows sunshine to occur only when the solar zenith angle is smaller than 94°, while in reality the upper part of the observed region is sunlit at even larger zenith angles.

4.2. Response to Solar Variability of the Diurnal Variation in Ozone at the Equator

[15] The response to solar variability of ozone diurnal variation at the equator obtained from HAMMONIA simulation is displayed in Figure 3. The response varies between

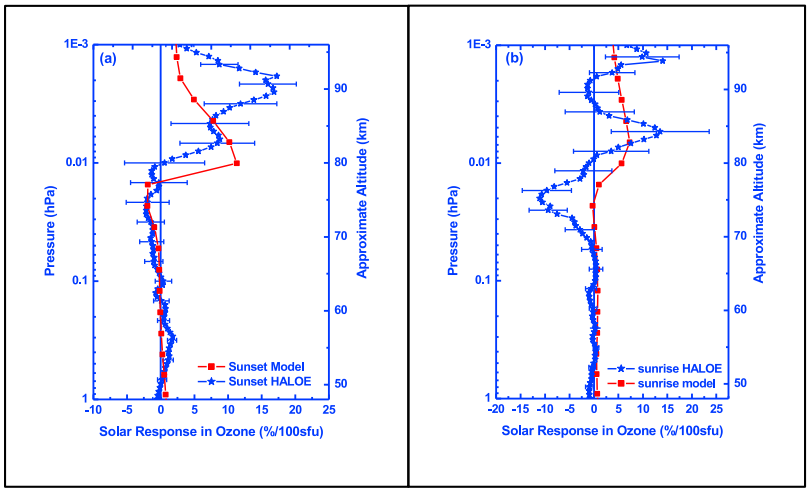

Figure 4. Vertical profiles of the solar response in ozone (%/100 sfu) near the equator as obtained from HALOE data (0–5°N) and the HAMMONIA model for (a) sunset time and (b) sunrise time. HAMMONIA results at the equator are for local times of 0600h and 1800h.

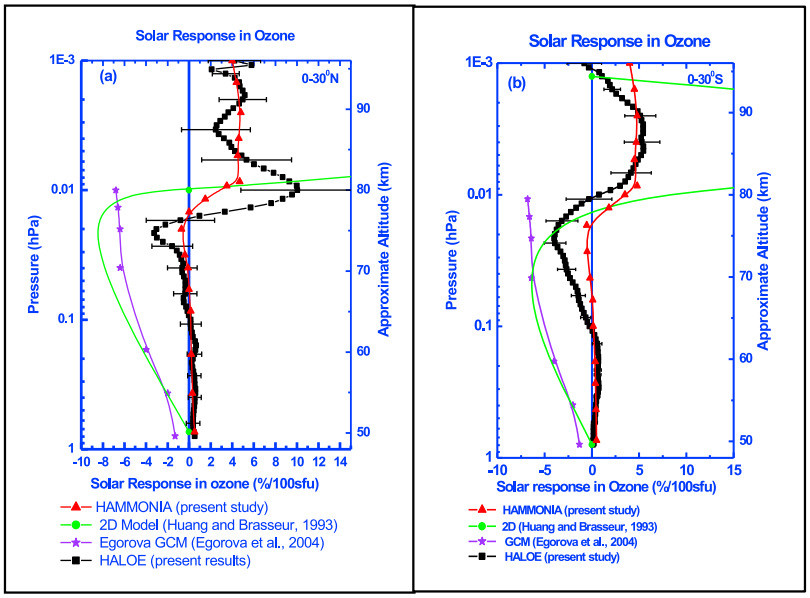

Figure 5. Response of ozone (%/100 sfu) to solar variability in the tropics (a) 0–30°N and (b) 0–30°S. In the case of HAMMONIA, zonal averages (meaning also an averaging over local times) are presented and compared to averages of sunrise and sunset data from HALOE.

−3%/100 sfu and +7%/100 sfu between 1 hPa (∼48 km) and 0.001 hPa (∼96 km) region. Strong positive response (7%/100 sfu) is observed between pressure levels 0.01 hPa (∼80 km) and 0.004 hPa (∼85 km) during 6–18 h. Strong negative response (∼1.3%/100 fsu) is observed near 0.02 hPa (∼75 km) during 9–15 hrs.

[16] As the absolute ozone values differ between sunrise and sunset, it can be expected that the solar response also does. *Marsh et al.* [2003] have analyzed trends from the same set of HALOE ozone observations and shown that sunrise and sunset trends differ significantly. The ozone response to solar cycle variability (in percent per 100 sfu) for sunrise and sunset is computed from HALOE data (averaged over 0–5°N belt) and from model simulations near the equator. The vertical profiles of the computed ozone response to solar variability for sunset and sunrise along with 2 sigma error bars are shown in Figures 4a and 4b respectively. There is good agreement between the model and experimental profiles in Figure 4a for the 50–75 km layer during the sunset period. Above 75 km, both model and experimental values indicate a sharp positive gradient. The HAMMONIA profile shows a maximum solar response of 12%/100 sfu around 80 km, which decreases with altitude and becomes 3% at about 95 km. The HALOE solar

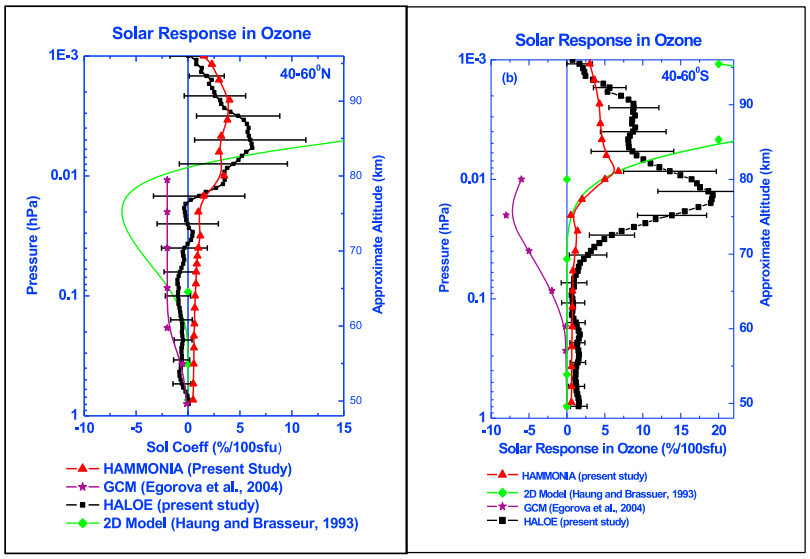

Figure 6. Response of ozone (%/100 sfu) to solar variability in midlatitudes (a) 40–60°N and (b) 40–60°S.

response exhibits a sharp gradient above 0.01 hPa with a value of 17%/100 sfu at around 90 km. The profiles shown in Figure 4b for sunset also indicate good agreement at lower heights but in the upper levels the agreement is relatively poor.

4.3. Ozone Response to Solar Variability in Four Latitude Bands

[17] Figures 5a and 5b show the variation with height of the ozone response as obtained from the HAMMONIA model and the HALOE observations in the 0–30°N and 0–30°S latitude belts respectively. These results are compared with earlier 2D [*Huang and Brasseur*, 1993] and General Circulation Model (GCM) [*Egorova et al.*, 2004] results. The agreement between observed and model results as obtained in the present work is quite reasonable for both hemispheres as evident from Figure 5. There are some minor differences that are discussed below. The agreement is excellent up to 0.0858 hPa (∼65 km) for the Southern hemispheric region and up 0.043 hPa (∼70 km) in the Northern Hemisphere. Near 70 km, the HALOE ozone response is negligible but becomes substantial at higher altitudes. Above these altitudes, the HALOE profile exhibits a higher solar response at some altitudes. In the 0–30°N belt, the HALOE profile is characterized by a peak of ∼10%/100 sfu near 0.01 hPa (∼80 km) while the solar response of ozone obtained from HAMMONIA simulation is ∼5%/100 sfu for the same pressure levels. In both latitudinal belts, the HALOE profile exhibits a minimum (3–5%/100 sfu) near 0.02 hPa (∼75 km), which is not observed in the HAMMONIA profile. General Circulation Models [*Egorova et al.*, 2004] and 2D models [*Huang and Brasseur*, 1993] simulations exhibit a negative ozone response of ∼2%/100 sfu near 0.794 hPa (∼50 km) which steadily increases to 7%/100 sfu (GCM) and 12%/100 sfu (2D-model) near 0.01 hPa (∼80 km). Above 0.01 hPa (∼80 km), the 2D model exhibits a strong positive ozone response with a peak of ∼40%/100 sfu near 0.0023 hPa (∼90 km).

[18] The ozone response to solar variability obtained from HAMMONIA and HALOE at 40–60°N and 40–60°S is shown in Figures 6a and 6b, respectively. In general, a positive response is observed in both belts in both the HALOE and HAMMONIA results. These observational and model results are compared earlier with 2D model [*Huang and Brasseur*, 1993] and MAECHAM4 spectral GCM [*Egorova et al.*, 2004] results. In both latitudinal belts, the vertical profile in the ozone response measured by HALOE exhibits similar variations as in the HAMMONIA model. The HALOE profile is in very good agreement with HAMMONIA up to 0.043 hPa (∼70 km) above which the HALOE profile is characterized by higher solar response values than the HAMMONIA profile at the same altitudes. The solar response obtained by HALOE below 0.02 hPa is found to be statistically insignificant in both hemispheres. Further, the 2-sigma error bars suggest that there is no significant variation in the middle and lower mesosphere. In fact, an inspection of the mean profiles in the ozone response highlights the differences between model and observations (real atmosphere). Note, however, that the GCM results are in relatively close agreement below 0.06 hPa. In the 40–60°S belt, the HALOE data exhibit a peak near 0.012 hPa (∼78 km) while the HAMMONIA profile shows a significant peak near 0.01 hPa (∼80 km). A peak is also observed in the 0–30°N belt at similar altitudes. Vertical profiles for the solar response of ozone obtained from 2D and GCM simulations are in very good agreement with HALOE and HAMMONIA profiles up to 0.0858 hPa (∼65 km), in both belts. In the 40–60°S belt, the 2D model profile is in very good agreement with the HAMMONIA profile up to 0.01 hPa (∼80 km). The agreement between HAMMONIA and HALOE is poor, however, around 0.02 hPa. In both belts, the 2D profile exhibits a strong positive (∼40–45%/100 sfu) ozone response near 0.0023 hPa (∼90 km), which is considerably higher than the response in HALOE and in HAMMONIA.

4.4. Diurnal Variation of Temperature at the Equator

[19] Figure 7 exhibits the diurnal variation of temperature at the equator as provided by HAMMONIA. The temperature is characterized by a small diurnal variation below 0.1 hPa, but by larger variations higher up in the mesosphere. The diurnal cycle in temperature is more evident when the temperature is presented as a deviation from the diurnal average (Figure 8). The diurnal cycle is clearly dominated by a migrating diurnal tidal structure with a peak-to-peak amplitude of about 20 K in the upper mesosphere. Earlier analyses of diurnal [*Achatz et al.*, 2008] and semi-diurnal [*Yuan et al.*, 2008; *Keckhut et al.*, 1996] tides produced by HAMMONIA indicate that, in general, the model reproduces reasonably well the observed tidal characteristics of the mesosphere and lower thermosphere.

4.5. Response to Solar Variability of the Diurnal Variation in Temperature at Equator

[20] Figure 9 shows that the calculated mesospheric response of temperature to increased solar flux (from minimum to maximum conditions) at the equator is positive. The response reaches maxima close to 2.7 K/100 sfu between 0.01 and 0.001 hPa depending on the local time. This time dependence becomes clearer in Figure 10 that shows local time-dependent anomalies of the temperature response calculated with respect to the diurnal average response at each pressure level. Above about 0.03 hPa, the temperature response shows a clear diurnal migrating tidal structure with maximum peak-to-peak amplitude of about 1 K. This suggests that the solar response can be interpreted as a modulation of the diurnal solar tide as presented in Figure 8. This is not surprising as the tide is partly excited by ozone heating in the stratosphere, which is itself modulated by changing solar activity.

4.6. Temperature Response to Solar Variability in Four Latitude Bands

[21] The responses in temperature to solar variability obtained from HAMMONIA and HALOE at 0–30°N and 0–30°S are shown in Figures 11a and 11b, respectively. These results are compared with earlier results from 2D models [*Fleming et al.*, 1995; *Arnold and Robinson*, 1998] and GCM [*Matthes et al.*, 2004] simulations in both latitudinal belts. The number of analyzed data points from HALOE in each latitudinal band is limited, so that a comparison with model results is not straightforward. Comparisons can therefore only be qualitative. Note that the model results appear to be quite systematic and follow a pattern without

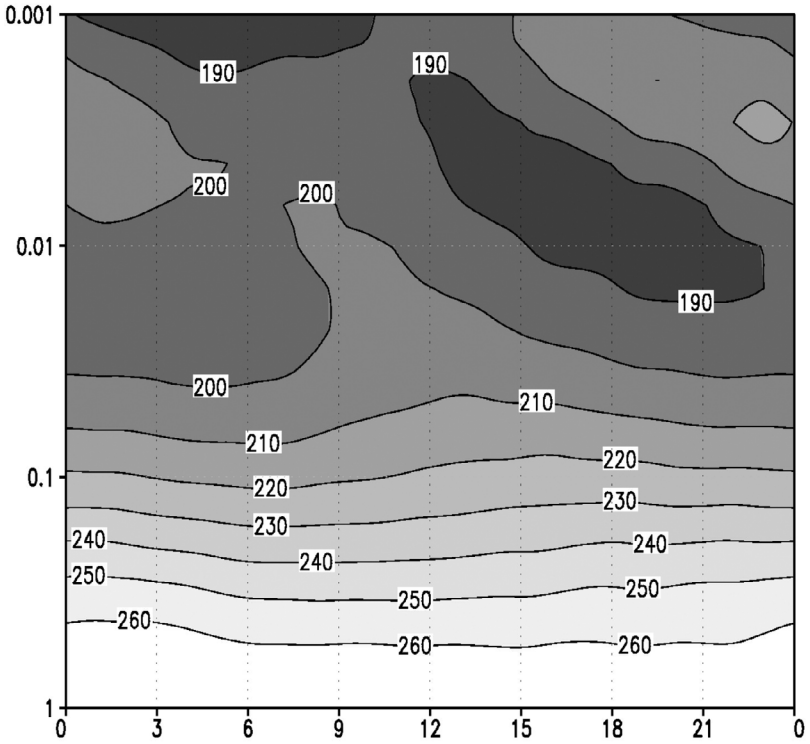

Figure 7. Diurnal variation in temperature (K) at the equator as simulated by HAMMONIA for solar minimum conditions. Axes: x axis denotes time (hours) and y axis denotes pressure (hPa).

any abrupt changes. Hence considering more points than provided by the HALOE coverage may not affect results significantly within the selected latitudinal bin. In both latitudinal belts, the HALOE profile is in good agreement with the HAMMONIA profile. In general a significant positive response (∼0.5–1.0 K/100 sfu) is observed except near 0.37 hPa (∼55 km) in the 0–30°S belt. These results are in agreement with the response obtained from 2D model, GCM simulations and rocketsonde observations. The 2D model [*Fleming et al.*, 1995] overestimates the temperature response above 0.043 hPa (∼70 km). The 2D model results of *Huang and Brasseur* [1993] also exhibit stronger a

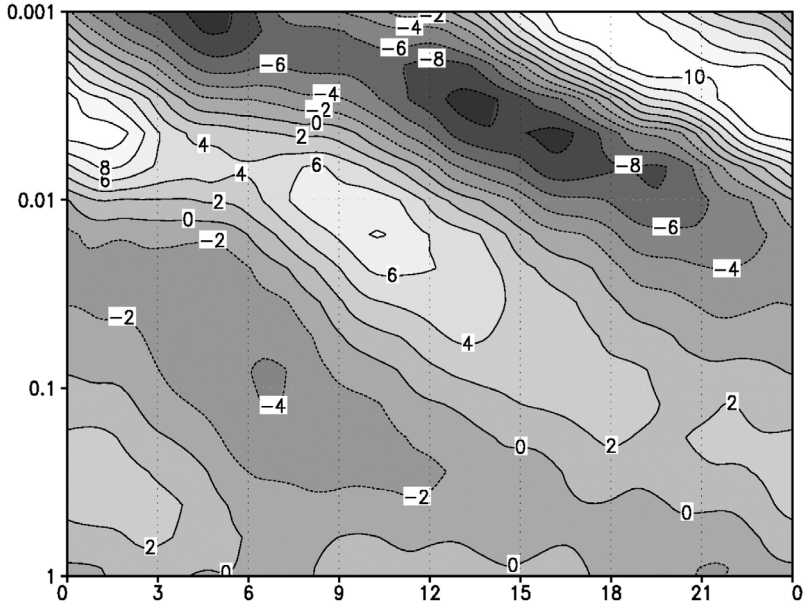

Figure 8. Diurnal variation in simulated temperature (K) at the equator as in Figure 7 but presented as anomalies (deviation from the diurnal average temperature). Axes: x axis denotes time (hours) and y axis denotes pressure (hPa).

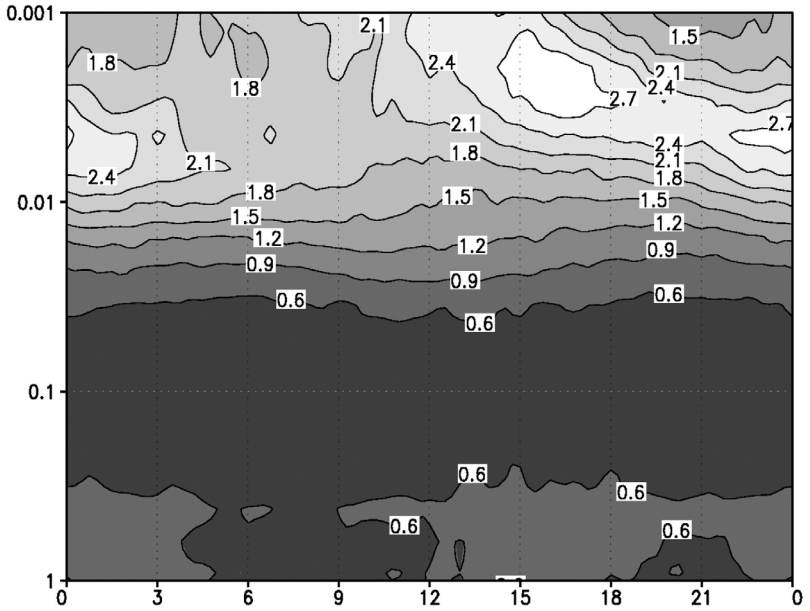

Figure 9. Diurnal variation in the response of temperature to solar variability (K/100 sfu) at the equator as simulated by HAMMONIA. Axes: x axis denotes time (hours) and y axis denotes pressure (hPa).

temperature response at the altitudes above 0.04 hPa (not included in Figure 11). In the 0–30°N belt, vertical profiles of HALOE and HAMMONIA agrees well with the vertical profile reported by *Fadnavis et al.* [2011]. The HALOE data indicates a solar signal of 1.0 ± 0.5 K/100 sfu around 80 km, which is statistically insignificant. The 2D models [*Fleming et al.*, 1995; *Huang and Brasseur*, 1993; *Arnold and Robinson*, 1998] overestimate the temperature response above 0.043 hPa (∼70 km). GCM simulations show negative temperature response above 0.0736 hPa (∼66 km). From rocketsonde data, *Keckhut et al.* [2005] reported a temperature response to solar cycle that is considerably higher (1.5–2 K/100 sfu) than the response derived from satellite observations. The reason may be that temperature response reported from rocketsonde temperatures corresponds to the Northern subtropics (Barking Sands, 22°N; Cape Kennedy, 28°N; Ponit Mugu, 34°N) whereas other results refer to the 0–30°N belt. From MAECHAM4 model simulations, *Egorova et al.* [2004] reported a response of temperature to solar variability varying from 0 and 1.2K between solar maximum and solar minimum in the atmospheric heights ranging from 1 to 0.01 hPa, and over the

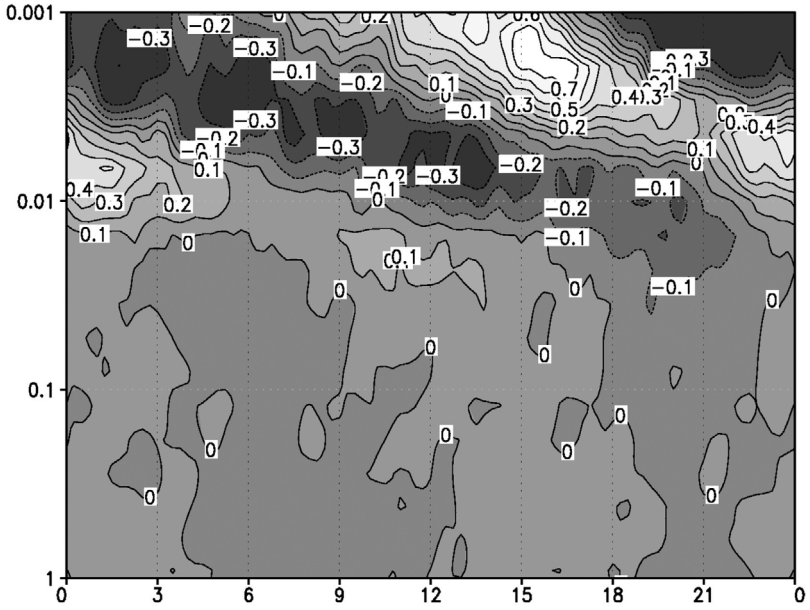

Figure 10. Diurnal variation in the simulated response of temperature to solar variability (K/100 sfu) at the equator as in Figure 9 but presented as anomalies (deviation from the diurnal average response). Axes: x axis denotes time (hours) and y axis denotes pressure (hPa).

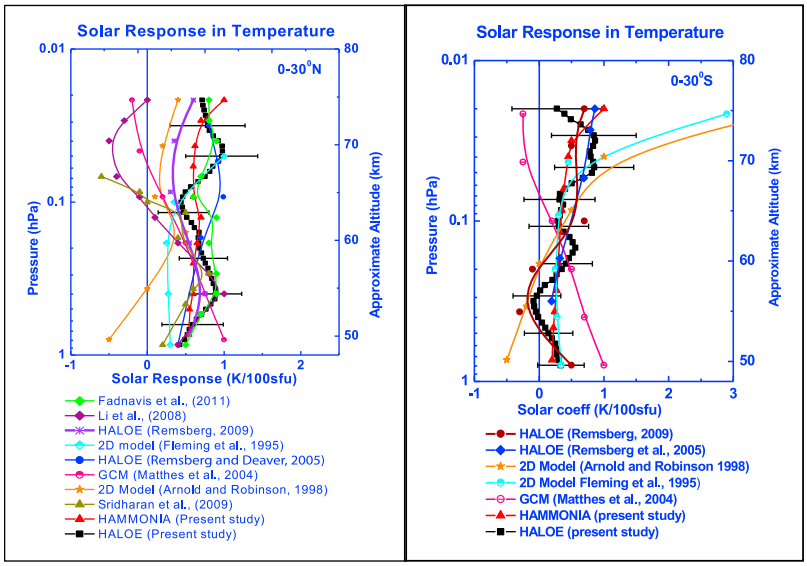

Figure 11. Response of temperature (K/100 sfu) to solar variability in the tropics (a) 0–30°N and (b) 0–30°S.

latitudinal belts of 0–30°N and 0–30°S. *Li et al.* [2008], *Sridharan et al.* [2009] and GCM results [*Matthes et al.*, 2004] show a negative temperature response to solar variability in the region between 0.2 hPa and 0.02 hPa. Vertical profiles of the response in HALOE temperature in both hemispheres obtained in the present study broadly agrees with the solar responses deduced from HALOE temperature by *Remsberg and Deaver* [2005]. Minor differences are observed at some pressure levels. As seen from the Figure 11a, the temperature response to solar variability as obtained by *Remsberg and Deaver* [2005] is of ∼1 K/100 sfu near 1 hPa, while it is equal to ∼0.4 K/100 sfu in the present study. Similarly, near 0.4 hPa, a temperature response of ∼0.5 K/100 sfu is derived in the present study, while it reaches ∼0.8 K/100 sfu in the analysis of *Remsberg and Deaver* [2005]. In the present study, the temperature response is computed in the 0–30° wide belt. Since *Remsberg and Deaver* [2005] reported temperature response for 10 degree-wide latitudinal belts we have averaged their results to the 0–30°N belt for comparison purposes. In the present work, we use the wider latitude belt to enhance the statistical robustness of the results. To increase the robustness of their results, *Remsberg and Deaver* [2005] have recently revisited the HALOE data and updated their results [*Remsberg*, 2009]. They again used the relatively small bin but apply another statistical technique.

[22] The temperature response to solar variability obtained from HAMMONIA and HALOE in 40–60°N and 40–60°S

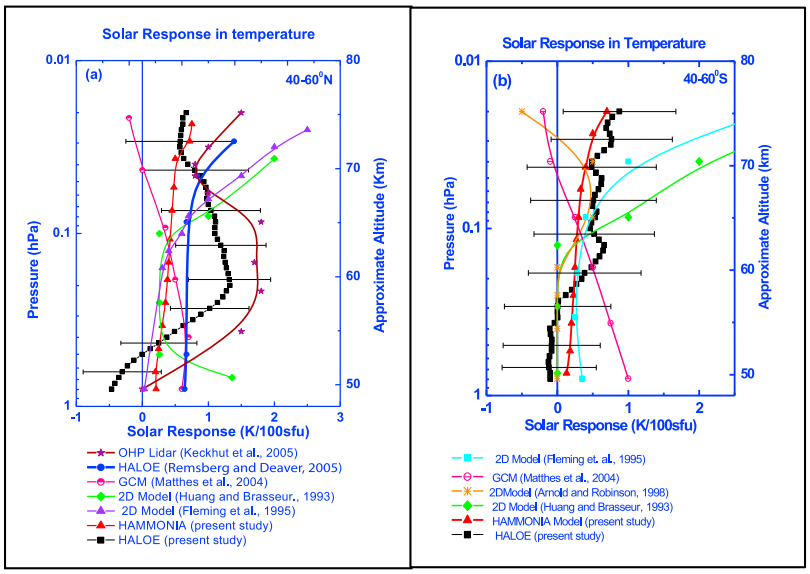

Figure 12. Response of temperature (K/100 sfu) to solar variability at midlatitudes (a) 40–60°N and (b) 40–60°S.

latitude ranges is shown in Figures 12a and 12b, respectively. These results are compared to 2D model simulations [*Fleming et al.*, 1995; *Arnold and Robinson*, 1998; *Huang and Brasseur*, 1993], GCM [*Matthes et al.*, 2004] in both latitudinal belts. HALOE temperatures exhibit a negative response to solar variability below 0.5 hPa (~53 km) in the Northern Hemispheric midlatitudes and below 0.369 hPa (~55 km) for the Southern hemispheric midlatitude. The response is positive above these altitudes. HAMMONIA simulations exhibit positive responses at all pressure levels between 0.794 hPa and 0.02 hPa in both belts. The HALOE data indicates a solar signal of 0.7 ± 0.7 K/100 sfu around 80 km, which is statistically insignificant. From their 2-D model simulations, *Arnold and Robinson* [1998] also reported a negative temperature response (0.5 K/100 sfu) at 40–60°N (figure not included). In the model study mentioned above, *Egorova et al.* [2004] reported temperature responses between ~0.3 and 0.9K between 1 and 0.01 hPa in the bands covering the 40–60°S and 40–60°N regions. In both latitudinal belts, 2D model simulations [*Huang and Brasseur*, 1993; *Fleming et al.*, 1995] overestimate the solar response above 0.43 hPa (~70 km). It is important to note that these models also overestimate the solar response in temperature in the 0–30°N-S belts.

5. Summary

[23] HALOE temperature and ozone measurements are used to investigate the 11-year solar signal in the mesosphere in the tropical and middle latitude regions of both hemispheres. Our analysis demonstrates that the annual response in ozone is statistically insignificant below 75 km altitude in the 0–30°N latitudinal belt and below 65 km in the 0–30°S belt. The annually averaged signal in ozone is found to be of the order of 5 to 10%/100 sfu with a peak at 80 km in the Northern Hemisphere. In most cases, the ozone response to solar variability deduced from HALOE measurements is in qualitative agreement with the response produced by the HAMMONIA model. A comparison with earlier published model results reveals that, in the lower part of the mesosphere, the response not only differs in magnitude but also in sign. At midlatitudes, the qualitative agreement between the model and HALOE ozone responses is found to be quite reasonable. However, a peak in the HALOE profile is found at 85 km (8%/100 sfu) in the 40–60°N latitudinal belt whereas at 40–60°S, a peak is found in the ozone response at 75 km (20%/100 sfu). No significant solar signal is found in the lower mesospheric ozone in both hemispheres. Agreement between the temperature response simulated by the model and derived from HALOE data is found to be rather good for low and midlatitudes. HALOE data indicates a temperature response to solar cycle variations that reach 0.5–1 K/100 sfu below 70 km and 1 K/100 sfu above 70 km in the tropics (both hemispheres). In the 40–60°N region, HALOE indicates a strong temperature response (1–1.5 K/100 sfu) in the middle mesosphere. The inferred solar signal in the temperature at 40–60°S is found to be 0.5 K/100 sfu but, in most cases, the signal is not significant. Model results agree well with experimental data in this region.

[24] In general, there is a reasonable agreement between the HAMMONIA model and HALOE results even though some significant differences exist. It should be stressed here that the different sampling method affects the results mainly in terms of statistical significance. Some differences may be attributed due to the selection of latitude sampling, but they are found to be marginal.

References

Achatz, U., N. Grieger, and H. Schmidt (2008), Mechanisms controlling the diurnal solar tide: Analysis using a GCM and a linear model, *J. Geophys. Res.*, *113*, A08303, doi:10.1029/2007JA012967.

Arnold, N. F., and T. R. Robinson (1998), Solar cycle changes to planetary wave propagation and their influence on the middle atmosphere circulation, *Ann. Geophys.*, *16*, 69–76, doi:10.1007/s00585-997-0069-3.

Austin, J., et al. (2008), Coupled chemistry climate model simulations of the solar cycle in ozone and temperature, *J. Geophys. Res.*, *113*, D11306, doi:10.1029/2007JD009391.

Banks, P. M., and G. Kockarts (1973), *Aeronomy, Part B*, Academic, San Diego, Calif.

Beig, G. (2000), The relative importance of solar activity and anthropogenic influences on the ion composition, temperature and associated neutrals of the middle atmosphere, *J. Geophys. Res.*, *105*, 19,841–19,856, doi:10.1029/2000JD900169.

Beig, G. (2002), Overview of the mesospheric temperature trend and factors of uncertainty, *Phys. Chem. Earth*, *27*, 509–519.

Beig, G., et al. (2003), Review of mesospheric temperature trends, *Rev. Geophys.*, *41*(4), 1015, doi:10.1029/2002RG000121.

Beres, J. H., R. R. Garcia, B. A. Boville, and F. Sassi (2005), Implementation of a gravity wave source spectrum parameterization dependent on the properties of convection in the Whole Atmosphere Community Climate model (WACCM), *J. Geophys. Res.*, *110*, D10108, doi:10.1029/2004JD005504.

Brasseur, G. (1993), The response of the middle atmosphere to long term and short-term solar variability: A two-dimensional model, *J. Geophys. Res.*, *98*, 23,079–23,090, doi:10.1029/93JD02406.

Brasseur, G., and S. Solomon (1986), *Aeronomy of the Middle Atmosphere*, 2nd ed., D. Reidel, Norwell, Mass.

Brühl, C., et al. (1996), Halogen Occultation Experiment ozone channel validation, *J. Geophys. Res.*, *101*(D6), 10,217–10,240, doi:10.1029/95JD02031.

Dikty, S., H. Schmidt, M. Weber, C. von Savigny, and M. G. Mlynczak (2010), Daytime ozone and temperature variations in the mesosphere: A comparison between SABER observations and HAMMONIA model, *Atmos. Chem. Phys.*, *10*, 8331–8339, doi:10.5194/acp-10-8331-2010.

Donnelly, R. F. (1991), Solar UV spectral irradiance variations, *J. Geomag. Geoelectr.*, *43*, 835–842, doi:10.5636/jgg.43.Supplement2_835.

Egorova, T., E. Rozanov, E. Manzini, M. Haberreiter, W. Schmutz, V. Zubov, and T. Peter (2004), Chemical and dynamical response to the 11-year variability of the solar irradiance simulated with a chemistry-climate model, *Geophys. Res. Lett.*, *31*, L06119, doi:10.1029/2003GL019294.

Fadnavis, S., G. Beig, and T. Chakraborti (2011), Decadal solar signal in ozone and temperature through the mesosphere of Northern tropics, *J. Atmos. Sol. Terr. Phys.*, doi:10.1016/j.jastp.2010.09.035, in press.

Fleming, L., S. Chandra, C. H. Jackman, D. B. Considine, and A. R. Douglass (1995), The middle atmospheric response to short and long term solar UV variations: Analysis of observations and 2D model results, *J. Atmos. Terr. Phys.*, *57*, 333–365, doi:10.1016/0021-9169(94)E0013-D.

Fomichev, V. I., and J.-P. Blanchet (1995), Development of the New CCC/GCM long wave radiation model for extension into the middle atmosphere, *Atmos. Ocean*, *33*, 513–529, doi:10.1080/07055900.1995.9649543.

Fomichev, V. I., J.-P. Blanchet, and D. S. Turner (1998), Matrix parameterization of the 15 μm CO_2 band cooling in the middle and upper atmosphere for variable CO_2 concentration, *J. Geophys. Res.*, *103*, 11,505–11,528, doi:10.1029/98JD00799.

Fomichev, V. I., W. E. Ward, S. R. Beagley, C. McLandress, J. C. McConnell, N. A. McFarlane, and T. G. Shepherd (2002), Extended Canadian Middle Atmosphere Model: Zonal mean climatology and physical parameterizations, *J. Geophys. Res.*, *107*(D10), 4087, doi:10.1029/2001JD000479.

Giorgetta, M. A., E. Manzini, and E. Roeckner (2002), Forcing of the quasi-biennial oscillation from a broad spectrum of atmospheric waves, *Geophys. Res. Lett.*, *29*(8), 1245, doi:10.1029/2002GL014756.

Hervig, M. E., et al. (1996), Validation of temperature measurements from the Halogen Occultation Experiment, *J. Geophys. Res.*, *101*, 10,277–10,285, doi:10.1029/95JD01713.

Hines, C. O. (1997a), Doppler-spread parameterization of gravity wave momentum deposition in the middle atmosphere. Part 1: Basic

formulation, *J. Atmos. Sol. Terr. Phys.*, *59*, 371–386, doi:10.1016/S1364-6826(96)00079-X.

Hines, C. O. (1997b), Doppler-spread parameterization of gravity wave momentum deposition in the middle atmosphere. Part 2: Broad and quasi monochromatic spectra, and implementation, *J. Atmos. Sol. Terr. Phys.*, *59*, 387–400, doi:10.1016/S1364-6826(96)00080-6.

Hong, S. S., and R. S. Lindzen (1976), Solar semidiurnal tide in the thermosphere, *J. Atmos. Sci.*, *33*, 135–153, doi:10.1175/1520-0469(1976)033<0135:SSTITT>2.0.CO;2.

Hood, L. (2004), Effects of solar UV variability on the stratosphere, in *Solar Variability and Its Effects on Climate*, *Geophys. Monogr. Ser.*, vol. 141, edited by J. M. Pap and P. Fox, pp. 283–303, AGU, Washington, D. C., doi:10.1029/141GM20.

Huang, T. Y. W., and G. P. Brasseur (1993), Effect of long-term solar variability in a two-dimensional interactive model of the middle atmosphere, *J. Geophys. Res.*, *98*, 20,413–20,427, doi:10.1029/93JD02187.

Keckhut, P., et al. (1996), Semi-diurnal and diurnal temperature tides (30–55 km): Climatology and effect on UARS-lidar data comparisons, *J. Geophys. Res.*, *101*, 10,299–10,310, doi:10.1029/96JD00344.

Keckhut, P., C. Cagnazzo, M.-L. Chanin, C. Claud, and A. Hauchecorne (2005), The 11-year solar-cycle effects on the temperature in the upper-stratosphere and mesosphere: Part I - Assessment of observations, *J. Atmos. Sol. Terr. Phys.*, *67*(11), 940–947, doi:10.1016/j.jastp.2005.01.008.

Kerzenmacher, T. E., P. Keckhut, A. Hauchecorne, and M. L. Chanin (2006), Methodological uncertainties in multi-regression analyses of middle-atmospheric data series, *J. Environ. Monit.*, *8*, 682–690, doi:10.1039/b603750j.

Khosravi, R., G. Brasseur, A. Smith, D. Rusch, S. Walters, S. Chabrillat, and G. Kockarts (2002), Response of the mesosphere to human-induced perturbations and solar variability calculated by a 2-D model, *J. Geophys. Res.*, *107*(D18), 4358, doi:10.1029/2001JD001235.

Kinnison, D. E., et al. (2007), Sensitivity of chemical tracers to meteorological parameters in the MOZART-3 chemical transport model, *J. Geophys. Res.*, *112*, D20302, doi:10.1029/2006JD007879.

Lean, J. (2000), Evolution of the Sun's spectral irradiance since the Maunder Minimum, *Geophys. Res. Lett.*, *27*, 2425–2428, doi:10.1029/2000GL000043.

Li, T., T. Leblanc, and I. S. McDermid (2008), Interannual variations of middle atmospheric temperature as measured by the JPL lidar at Mauna Loa Observatory, Hawaii (19.5°N, 155.6°W), *J. Geophys. Res.*, *113*, D14109, doi:10.1029/2007JD009764.

Lin, S. J., and R. B. Rood (1996), Multidimensional flux-form semi-Lagrangian transport schemes, *Mon. Weather Rev.*, *124*, 2046–2070, doi:10.1175/1520-0493(1996)124<2046:MFFSLT>2.0.CO;2.

Manzini, E., N. A. McFarlane, and C. McLandress (1997), Impact of the Doppler spread parameterization on the simulation of the middle atmosphere circulation using the MA/ECHAM4 general circulation model, *J. Geophys. Res.*, *102*, 25,751–25,762, doi:10.1029/97JD01096.

Marsh, D., A. Smith, and E. Noble (2003), Mesospheric ozone response to changes in water vapor, *J. Geophys. Res.*, *108*(D3), 4109, doi:10.1029/2002JD002705.

Matthes, K., U. Langematz, L. J. Gray, K. Kodera, and K. Labitzke (2004), Improved 11-year solar signal in the Freie Universität Berlin Climate Middle Atmosphere Model (FUB-CMAM), *J. Geophys. Res.*, *109*, D06101, doi:10.1029/2003JD004012.

Neter, J., W. Wasserman, and M. H. Kunter (1985), *Applied Linear Statistical Models*, 2nd ed., 1127 pp., Richard D. Irwin, Homewood, Ill.

Randel, W. J., and J. B. Cobb (1994), Coherent variations of monthly mean total ozone and lower stratospheric temperature, *J. Geophys. Res.*, *99*, 5433–5447, doi:10.1029/93JD03454.

Remsberg, E. E. (2009), Trends and solar cycle effects in temperature versus altitude from the Halogen Occultation Experiment for the mesosphere and upper stratosphere, *J. Geophys. Res.*, *114*, D12303, doi:10.1029/2009JD011897.

Remsberg, E. E., and L. E. Deaver (2005), Interannual, solar cycle, and trend terms in middle atmospheric temperature time series from HALOE, *J. Geophys. Res.*, *110*, D06106, doi:10.1029/2004JD004905.

Remsberg, E., et al. (2002), An assessment of the quality of Halogen Occultation Experiment temperature profiles in the mesosphere based on comparisons with Rayleigh backscatter Lidar and inflatable falling sphere measurements, *J. Geophys. Res.*, *107*(D20), 4447, doi:10.1029/2001JD001521.

Richards, P. G., J. A. Fennelly, and D. G. Torr (1994), EUVAC: A solar EUV Flux model for aeronomic calculations, *J. Geophys. Res.*, *99*, 8981–8992, doi:10.1029/94JA00518.

Roeckner, E., et al. (2003), The atmospheric general circulation model ECHAM 5. Part I: Model description, *Tech. Rep. 349*, MPI for Meteorol., Hamburg, Germany.

Roeckner, E., R. Brokopf, M. Esch, M. Giorgetta, S. Hagemann, L. Kornblueh, E. Manzini, U. Schlese, and U. Schulzweida (2006), Sensitivity of simulated climate to horizontal and vertical resolution in the ECHAM5 atmosphere model, *J. Clim.*, *19*, 3771–3791, doi:10.1175/JCLI3824.1.

Rozanov, E. V., M. E. Schlesinger, T. A. Egorova, B. Li, N. Andronova, and V. A. Zubov (2004), Atmospheric response to the observed increase of solar UV radiation from solar minimum to solar maximum simulated by the Univ. of Illinois at Urbana-Champaign climate-chemistry model, *J. Geophys. Res.*, *109*, D01110, doi:10.1029/2003JD003796.

Russell, J. M., III, L. L. Gordley, J. H. Park, S. R. Drayson, D. H. Hesketh, R. J. Cicerone, A. F. Tuck, J. F. Frederick, J. E. Harries, and P. J. Crutzen (1993), The Halogen Occultation Experiment, *J. Geophys. Res.*, *98*, 10,777–10,797, doi:10.1029/93JD00799.

Scaife, A., J. Austin, N. Butchart, S. Pawson, M. Keil, J. Nash, and I. N. James (2000), Seasonal and interannual variability of the stratosphere diagnosed from UKMO TOVS analyses, *Q. J. R. Meteorol. Soc.*, *126*, 2585–2604, doi:10.1002/qj.49712656812.

Schmidt, H., and G. P. Brasseur (2006), The response of the middle atmosphere to solar cycle forcing in the Hamburg model of the neutral and ionized atmosphere, *Space Sci. Rev.*, *125*(1–4), 345–356.

Schmidt, H., G. P. Brasseur, M. Charron, E. Manzini, M. A. Giorgetta, V. I. Fomichev, D. Kinnison, D. Marsh, and S. Walters (2006), The HAMMONIA chemistry climate model: Sensitivity of the mesopause region to the 11-year solar cycle and CO_2 doubling, *J. Clim.*, *19*, 3903–3931, doi:10.1175/JCLI3829.1.

She, C. Y., and D. A. Krueger (2004), Impact of natural variability in the 11-year mesopause region temperature observation over Fort Collins, CO (41°N, 105°W), *Adv. Space Res.*, *34*, 330–336, doi:10.1016/j.asr.2003.02.047.

Simmons, A. J., D. M. Burridge, M. Jarraud, C. Girard, and W. Wergen (1989), The ECMWF medium-range prediction models: Development of the numerical formulations and the impact of increased resolution, *Meteorol. Atmos. Phys.*, *40*, 28–60, doi:10.1007/BF01027467.

Sridharan, S., P. V. Prasanth, and Y. B. Kumar (2009), A report on long term trends and variabilities in middle atmospheric temperature over Gadanki (13.5°N, 79.2°E), *J. Atmos. Sol. Terr. Phys.*, *71*, 1463–1470, doi:10.1016/j.jastp.2008.09.017.

Thuillier, G., and S. Bruinsma (2001), The Mg II index for upper atmosphere modeling, *Ann. Geophys.*, *19*, 219–228, doi:10.5194/angeo-19-219-2001.

Weatherhead, E. C., A. J. Stevermer, and B. E. Schwartz (2002), Detecting environmental changes and trend, *Phys. Chem. Earth*, *27*, 399–403.

Woods, T. N., and G. J. Rottman (1997), Solar Lyman-alpha irradiance measurements during two solar cycles, *J. Geophys. Res.*, *102*, 8769–8779, doi:10.1029/96JD03983.

Yuan, T., H. Schmidt, C. Y. She, D. A. Krueger, and S. Reising (2008), Seasonal variations of semidiurnal tidal perturbations in mesopause region temperature, zonal and meridional winds above Fort Collins, CO (40.6°N, 105°W), *J. Geophys. Res.*, *113*, D20103, doi:10.1029/2007JD009687.

G. Beig and S. Fadnavis, Physical Meteorology and Aerology Division, Indian Institute of Tropical Meteorology, Dr. Homi Bhabha Road, Pashan Pune 411008, Pune, India. (suvarna@tropmet.res.in)

G. P. Brasseur, Climate Service Center, Chilehaus - Eingang B, Fischertwiete 1, D-20095 Hamburg, Germany.

H. Schmidt, Atmosphere in the Earth System, Max Planck Institute for Meteorology, Bundesstrasse 53, D-20255 Hamburg, Germany.